Journal of Science and Technology – Engineering and Technology for Sustainable Development
Volume 36, Issue 3, July 2026, 054–060

The Influence of Temperature on the Shape, Quality, and Activity of the Recycled Oyster Shell Catalyst for the Oxidative Coupling of Methane Process

Dao Xuan Bach, Nguyen Thanh Hung, Le Minh Thang*, Bui Minh An
Hanoi University of Science and Technology, Ha Noi, Vietnam
Corresponding author email: thang.leminh@hust.edu.vn

Abstract

Hundreds of catalysts have been explored and developed for the oxidative coupling of methane process, most of which come from commercial chemicals, rare metals, and expensive materials that are not available and contain toxic chemicals. With the richness of nature, sources from biomass and sustainable materials are gradually being developed as substitutes. This work focuses on the conditions for synthesizing CaO from oyster shells, an abundant and available raw material, as well as a waste source that has not yet been fully utilized. The catalysts synthesized from these oyster shells were treated under different conditions to produce materials with different characteristics. All synthesized catalysts from oyster shells have a higher selectivity for hydrocarbons than the commercial CaO powder. Oyster shells heated up to 950 °C under continuous air flow were the most active catalyst, achieving a hydrocarbon selectivity of approximately 70.3% when the reaction was carried out at 750 °C. This exceptional selectivity comes from the strong basicity available in oyster shells, which increases the oxygen mobility and easily helps react. The catalysts were also evaluated for stability at 750 °C for 225 min with good results.

Keywords: Alkali metals, catalysts, methane, oyster shells, sustainable source.

1. Introduction

Methane is an abundant and common gas in nature and can be found in large quantities in coal mines, industrial livestock operations, oil and gas mines, etc. However, most of the methane deposits are in sparsely populated areas, making it economically unfeasible to transport the gas [1]. On the other hand, methane is classified as a greenhouse gas and an agent perpetrating approximately 30% of the increase in average temperatures around the world [2]. Therefore, reducing methane emissions and utilizing it more sustainably present a significant opportunity to mitigate the near-term effects of climate change [2]. Since the 1970s, there has been a growing need to convert methane on a wide scale and on-site into transportable high-density energy sources or high-value-added chemicals such as hydrogen, olefins, and aromatics [1].

Currently, commercial methane conversion processes almost follow the path of indirect conversion; this intermediate path is the process of converting methane into syngas (H_2 and CO). Syngas, once formed, is used in the processes of methanol synthesis [3] and Fischer-Tropsch synthesis [4] to manufacture diverse compounds such as olefins, methanol, and synthetic fuels. Indirect methane conversion is only possible with a big investment because it requires making syngas, which uses a lot of energy. Direct conversion of methane into ethylene is currently one of the most potential options because it produces the high-value product while saving money and energy for the manufacturing process [5]. In 1982, there were two scientists, Keller and Bhasin, who pioneered the study of the oxidative coupling of methane (OCM) process [6]. The most notable and useful product of the OCM process is ethylene (C_2H_4). With its important physicochemical properties, ethylene is the most widely used olefin in the petrochemical organic synthesis industry to produce precious and varied products with high economic efficiency [1]. Therefore, the successful conversion of methane into ethylene with high efficiency is highly anticipated in the future. Global reactions for OCM process reported by Stansch *et al.* [7] were shown below:

$2O_2 + CH_4 \rightarrow 2H_2O + CO_2$ $\quad \Delta H^0_{298} \approx$ -802 kJ

$\frac{1}{2}O_2 + 2CH_4 \rightarrow H_2O + C_2H_6$ $\quad \Delta H^0_{298} \approx$ -177 kJ

$O_2 + CH_4 \rightarrow H_2O + CO + H_2$ $\quad \Delta H^0_{298} \approx$ -277 kJ

$\frac{1}{2}O_2 + CO \rightarrow CO_2$ $\quad \Delta H^0_{298} \approx$ -283 kJ

$\frac{1}{2}O_2 + C_2H_6 \rightarrow H_2O + C_2H_4$ $\quad \Delta H^0_{298} \approx$ -105 kJ

$2O_2 + C_2H_4 \rightarrow 2H_2O + 2CO$ $\quad \Delta H^0_{298} \approx$ -757 kJ

p-ISSN 3093-3242
e-ISSN 3093-3579
https://doi.org/10.51316/jst.191.etsd.2026.36.3.8
Received: May 5, 2025; Revised: Oct 9, 2025
Accepted: Oct 9, 2025; Online: May 26, 2026

$C_2H_6 \rightarrow H_2 + C_2H_4$ $\Delta H_{298}^0 \approx +137$ kJ

$C_2H_4 + 2H_2O \rightarrow 2CO + 4H_2$ $\Delta H_{298}^0 \approx +210$ kJ

$CO + H_2O \rightarrow CO_2 + H_2$ $\Delta H_{298}^0 \approx -41$ kJ

$CO_2 + H_2 \rightarrow CO + H_2O$ $\Delta H_{298}^0 \approx +41$ kJ

Hundreds of catalysts for the OCM reaction have been investigated, consisting of rare-earth metal oxides, alkaline earth metal oxides, and other complex metal catalysts [5], but most of them are synthesized from commercial chemical sources. Alkaline metal oxide is one of the first catalysts to be studied for the OCM process in the early 1990s. CaO could be the potential catalyst for this group of catalysts for alkaline metal oxides. An *et al.* [8] used CaO powder prepared by the decomposition of calcium nitrate at 700 °C in air for a study, achieving methane conversion and C_2^+ selectivity of 40% and 50%, respectively, at 800 °C with a CH_4/O_2/He flow rate of 8/2/10 ml · min^{-1}. In 2020, Lima *et al.* [9] published an article on synthesizing CaO from eggshells for use as a catalyst for the OCM process. That study reported that both methane conversion and C_2^+ selectivity had high values, approximately 30% and 56%, respectively.

The conversion of biological waste into high-value-added products is currently a hot topic in the study. In 2023, the worldwide oyster market reached 7.3 million tons. According to the IMARC Group, the market will reach 8.7 million tons by 2032, with a 2% compound annual growth rate (CAGR) from 2024 to 2032 [10]. As a result, a large number of oyster shells will be disposed of, occupying land resources, and solid waste will accumulate, polluting the soil and marine environment. Recycling these waste oyster shells is supposed to be expected to bring sustainable benefits. Some important fields, such as wastewater treatment and regenerative medicine, used oyster shells for converting to calcium carbonate ($CaCO_3$) to limit the exploitation of other unsustainable raw materials. The oyster shell contains approximately 95% $CaCO_3$ [11]; therefore, it can be considered a sustainable source of raw material to produce CaO powder for the OCM process.

2. Experimental Procedures

2.1. Catalyst Preparation

Oyster shells (OSs) in CatBa Island, Vietnam, were used to synthesize catalysts under different conditions. These shells were washed with water and some waste, then they were dried in the drying cabinet at 120 °C. After that, the material was heat-treated up to 200 °C to further clean the surface before being fed into a ball mill (MRC Scientific Instruments) for 5 min and labeled as OSs. Finally, the material was calcined at 950 °C with a ramping temperature rate of 10 °C min^{-1} under the following conditions: (1) for 0h in a furnace labeled OSs_0h, (b) for 1h in a furnace labeled OSs_1h, and (c) for 0h in a tube furnace with an air flow rate of 100 ml · min^{-1} labeled Air/OSs_0h.

2.2. Catalyst Characterization

The calcining temperature survey and prediction of the main speciation of OSs powder was carried out by thermogravimetric analysis (TGA) using the STA 449 Fx Jupiter 50571 device/Version 1.6 eco/November 2021 of NETZSCH. It was used to analyze the sample from 25 ℃ to 950 ℃ with a ramping temperature rate of 10 °C · min^{-1}.

Powder X-ray diffraction (XRD) was used to confirm the crystalline structures of the produced catalysts via the D8 Advance Bruker device using CuKα radiation.

Scanning electron microscopy (SEM), energy-dispersive X-ray spectroscopy (EDS), and elemental mapping were used in the JEOL JCM-7000 machine (Japan) to perform quantitative analysis of elemental composition and observe the surface of all the samples at a voltage of 15 kV.

Fourier transform infrared spectroscopy (FT-IR) was utilized to evaluate catalytic characteristics and determine the functional group present in the material to be more certain about its speciation. The measurement was conducted in the 400 – 4000 cm^{-1} range with a step size of 1 cm^{-1} using an ATR mode of the Nicolet iS50 FT-IR spectrometer.

The samples were also characterized by using the Brunauer-Emmett-Teller (BET) equation to evaluate the specific surface area on the Micromeritics Gemini VII system.

2.3. Catalyst Testing

After pelleting the catalysts and grinding them into particles (dp = 200 – 450 μm), 0.2 g of catalyst was loaded into the quartz tube (370 mm height, 5 mm ID), the catalyst was supported and fixed between two layers of quartz wool in the middle area of the tube. The catalyst tube was placed in the center of a continuous flow fixed-bed reactor. The reactor feed was mixed from two gas cylinders (35 v/v% CH_4/N_2 and 20 v/v% O_2/N_2) with a ratio of CH_4:O_2 (v/v) equal 4:1. The gas flow rate was adjusted on the Ablloge device; the total flow rate was 34.5 ml · min^{-1}, and a gas hourly space velocity was calculated with a result of 16500 h^{-1}. The reactor was heated to 650 ℃, 700 ℃, and 750 ℃ for catalytic experiments. The water vapor from the reaction was naturally cooled and removed from the gas products by a liquid trap.

The gas products were constantly checked by gas chromatography (GC) device with a flame ionization detector (FID) and another GC device with a thermal conductivity detector (TCD). The schematic diagram of the OCM experiment setup is depicted in Fig. 1.

The formula utilized for calculating CH_4 conversion (1), C_2 selectivity (2), and C_3H_6 selectivity (4) is shown below:

$$\text{CH}_4 \text{ conversion (\%)} = \frac{\%CH_{4before} - \%CH_{4after}}{\%CH_{4before}} \quad (1)$$

$$\text{C}_2 \text{ selectivity (\%)} = \frac{\%C_2H_4 + \%C_2H_6}{\%C_2H_4 + \%C_2H_6 + \%C_3H_6 + \%CO_x} \quad (2)$$

$$\text{C}_2\text{H}_x \text{ selectivity (\%)} = \frac{\%C_2H_x}{\%C_2H_4 + \%C_2H_6 + C_3H_6 + \%CO_x} \quad (3)$$

$$\text{C}_3\text{H}_6 \text{ selectivity (\%)} = \frac{\%C_3H_6}{\%C_2H_4 + \%C_2H_6 + C_3H_6 + \%CO_x} \quad (4)$$

where:

$\%CH_4$, $\%C_2H_4$, $\%C_2H_6$, $\%C_3H_6$, $\%CO_x$: Molar concentration of gases (%).

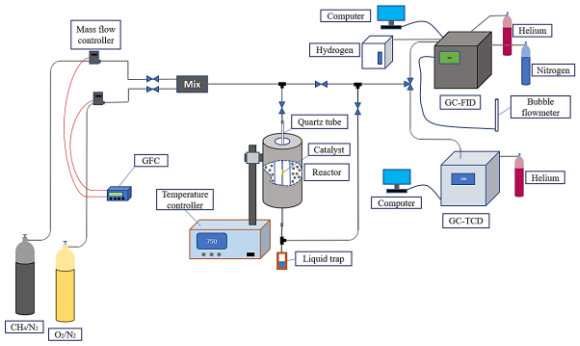

Fig. 1. The schematic diagram of the oxidative coupling of the methane process at the GeViCat center

3. Results and Discussion

3.1. Catalyst Characterization

Fig. 2 shows the thermal analysis results of oyster shells, which were heated from 25 °C to 950 °C at a ramping temperature rate of 10 °C · min^{-1} in both N_2 (50 ml · min^{-1}) and air (50 ml · min^{-1}) to observe changes in mass. The results shown in the derivative thermogravimetric (DTG) curve correspond to the endothermic process and decomposition of calcium carbonate ($CaCO_3$) into calcium oxide (CaO) [12]. First, there is a small change from 25 °C to 200 °C; this is due to the dehydration process of the material. However, the material was dried at 200 °C in the pretreatment, so the mass loss here is insignificant. In the next stage from 200 °C to about 600 °C, the mass of OSs decreased by 1.87%, which may be due to the decomposition of easily degradable organic compounds or the loss of chemically bound water inside the material. Theoretically, CO_2 accounts for about 44% of the weight of $CaCO_3$. The DTG curve shows a rapid mass loss after 600 °C. At 835 °C, the maximum mass loss was recorded as 41.69%, which is close to the theoretical CO_2 content. Therefore, the pyrolysis of OSs has been completed, forming CaO. It can be confirmed that most of the oyster shells converted to CaO at 950 °C.

The results of energy-dispersive X-ray spectroscopy (EDS) analysis and surface area of all samples are recorded in Table 1 (for ease of comparison, some elements with small contents are omitted, such as Na, Mg, Cl, and S, which are not listed in Table 1). The Ca/O atomic composition ratio was monitored and showed that for samples calcined at 950 °C, the Ca/O ratio was higher than that of oyster shells heat-treated at 200 °C. This result is consistent with the DTG analysis results because below 200 °C, no reaction processes occurred on the material, especially the decomposition of calcium carbonate. The samples calcined at 950 °C all gave Ca/O ratios close to the theoretical value Ca/O equal 1.

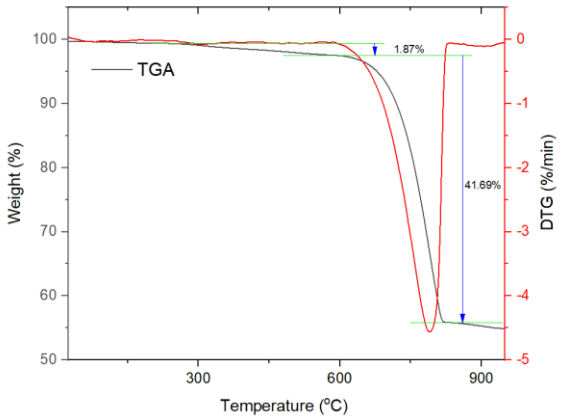

Fig. 2. Thermogravimetric analysis (TGA) and DTG curve for Oyster shells (OSs)

Table 1. The results of energy-dispersive X-ray spectroscopy analysis and BET Surface area

Sample	% Atom			Ca/O ratio	Surface area (m^2/g)
	Ca	O	C		
OSs	18.5	59.9	20.9	0.3	4.91
OSs_0h	52.3	43.3	-	1.2	0.67
OSs_1h	40.9	52.2	-	0.8	0.65
Air/OSs_0h	41.5	49.5	-	0.8	2.59
Chinese CaO	-	-	-	-	4.23

The samples also showed low specific surface area (Table 1). Initially, after heat treatment at 200 °C and grinding, OSs gave a surface area of 4.91 m^2/g. However, after calcination at 950 °C, the samples gave a specific surface area of less than 1 m^2/g. This may be due to the high-temperature calcination that has caused them to be sintered. In particular, the Ari/OSs_0h sample gave the best specific surface area among the samples calcined at 950 °C, reaching 2.59 m^2/g. It is implied that the presence of airflow provided oxygen, creating favorable conditions for the combustion process, thereby increasing the specific surface area and preventing the sintering process from occurring, increasing the specific surface value.

The SEM images of the samples are shown in Fig. 3. The oyster shell has a porous surface, consisting of many small particles stuck together to form clusters. Fig. 3a shows that OSs has a shape like a cotton bundle, with small cotton-like fragments. However, after being treated at high temperatures, the three samples treated at 950 °C are mainly in the form of blocks. Among them, the samples OSs_0h, and OSs_1h (Fig. 3b and Fig. 3c) have larger blocks that are not uniform in size from 2 – 5 µm and have the phenomenon of sintering together. In particular, the sample treated with oxygen (Fig. 3d) has a clear cubic shape and does not sinter into large blocks; the particles are much smaller and more uniform than the two samples treated in the static furnace, reaching a size of 0.5 – 1 µm. Fig. 3e is an SEM image of the Ari/OSs_0h sample at 50,000x magnification, clearly showing the morphology and particle size. These particles are evenly distributed and discrete, not agglomerated. The estimated size of these quadrilaterals is less than 1000 nm. This result is consistent with the specific surface area of the samples in Table 1.

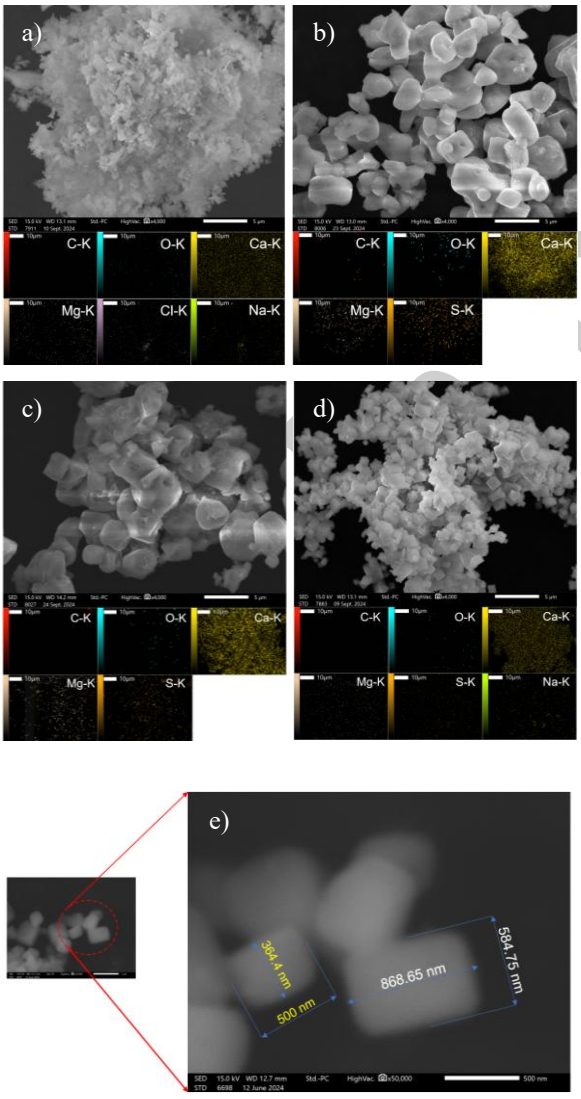

Fig. 3. The SEM-Mapping observation of catalysts: (a) OSs, (b) OSs_0h, (c) OSs_1h, (d and e) Air/OSs_0h

The elemental mappings of the materials in this work are shown in Fig. 3. It is clear that in addition to the existence of the three main elements (C, O, and Ca), oyster shells also contain elements such as Na, Mg, Cl, and S. The mapping results for each element demonstrate that the elements are quite uniform across the surface of the samples. Among them, Ca and O account for the largest density on the map. Fig. 3b and Fig. 3c did not show the elements Na and Cl that were seen in the OSs sample. This could be because there was too small of an amount of Na and Cl on the surface of OSs_0h and OSs_1h. In addition, the absence of these elements may be due to the molten sodium chloride (NaCl) salt at around 801 °C [13], which leads to the formation of other particles that crystallize outside the active region or the evaporation of Cl gas at high temperatures. According to some sources, the presence of metals such as magnesium (Mg) and sodium (Na) is particularly helpful for the selective oxidation of methane [14, 15].

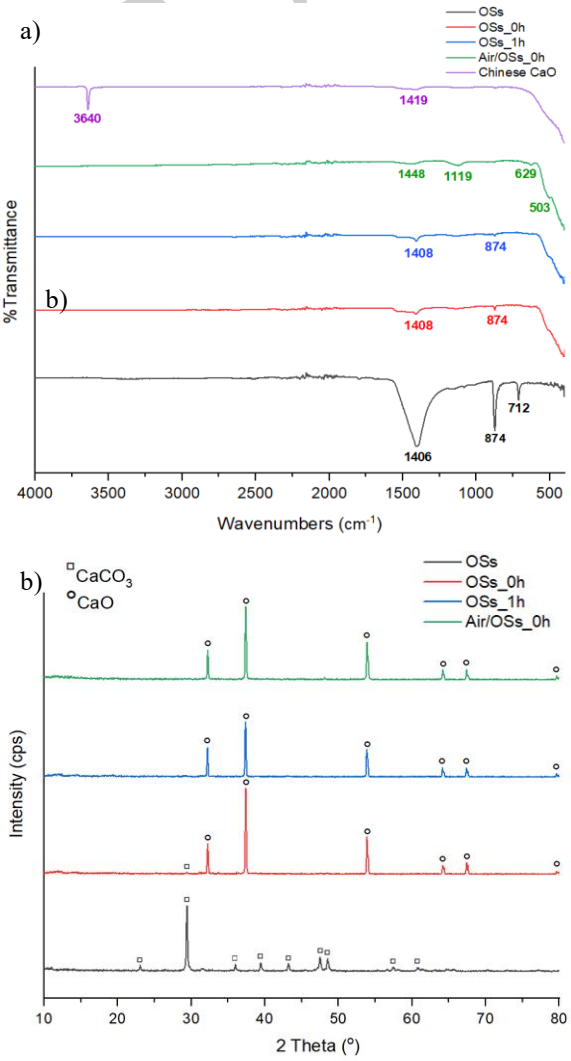

Fig. 4. The FT-IR analysis results (a) and the XRD pattern analysis results (b)

The FT-IR and XRD patterns are shown in Fig. 4. According to the FT-IR data, it shows that OSs with the most intense bands: 712 cm^{-1}, 874 cm^{-1}, and 1406 cm^{-1}, are the FT-IR spectrum of $CaCO_3$ [16]. Calcite characteristics are able to be observed at (ν_4) 712 cm^{-1} and (ν_2) 874 cm^{-1}. Calcite exhibits two absorption bands: out of the bending plane (ν_2) and doubly degenerate planar bending (ν_4) [17]. Two samples that were treated by oven at 950 °C still had bands: (ν_2) 874 cm^{-1}, 1408 cm^{-1} with lower signals than OSs, showing that there is still $CaCO_3$ in the composition, but not much. The absence of a significant absorption peak at 1406 cm^{-1} of the Air/OSs_0h sample indicates that the fundamental component of oyster shells, $CaCO_3$, has been transformed into CaO. The band at 503 cm^{-1} identified the vibration of the Ca–O band [18]. Regarding the XRD pattern, the OSs sample has the appearance of characteristic planes for $CaCO_3$ such as (012), (104), (110), (113), (202), (018), and (016) [16]. After the oyster shell was calcined at 950 °C on the samples, the characteristic diffraction peaks of $CaCO_3$ were replaced by diffraction peaks of CaO at 32.2°, 37.3°, 58.9°, 64.2°, and 67.3°, respectively (Fig. 4b) [9]. However, for the sample (OSs_0h), there was still a small peak of $CaCO_3$, indicating that the decomposition process of $CaCO_3$ to form CaO had not occurred completely. On the samples (OSs_1h) and (Air/OSs_0h), this was not recorded, indicating that the pyrolysis process had occurred completely to form CaO, the sharp peaks without strange peaks showed high crystallinity.

3.2. Catalyst Testing

The samples were carried out the reaction at 650 °C, 700 °C, and 750 °C as shown in Fig. 1 obtained the following results:

CH_4 conversion at different reaction temperatures was shown in Fig. 5a. It could be seen that the CH_4 conversion increased with increasing temperature and achieved the most outstanding value at 750 °C in the surveyed range. Two samples that reached the highest CH_4 conversion were the Chinese CaO and the Air/OSs_0h with values of 13.78% and 13.49%, respectively. This result is suitable with the BET result because the Chinese CaO had S_{BET} of 4.23 m^2/g and the Air/OSs_0h had S_{BET} of 2.59 m^2/g, which are higher than the values of the other samples. Besides, although the BET and elemental mapping analysis results for both OSs_0h and OSs_1h were almost identical, the OSs_0h had the lowest CH_4 conversion because the decomposition process of $CaCO_3$ was incomplete, which might negatively influence the reaction; this was shown in the FTIR and XRD result in Fig. 4. Therefore, the surface area might greatly affect the CH_4 conversion. The OSs samples had low CH_4 conversion, possibly due to the existence of alkali metals (Na and Mg), which was indicated in Rane's study [15].

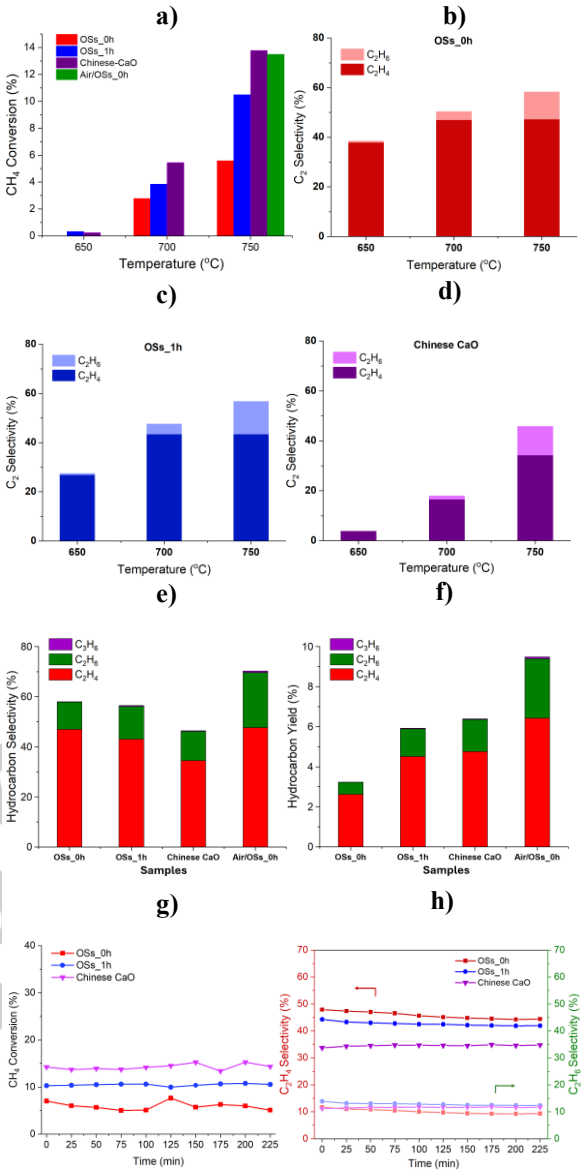

Fig. 5. The results of carrying out the OCM with catalysts in this work and Chinese CaO: (a) CH_4 conversion of samples; (b) C_2 product selectivity by temperature of OSs_0h; (c) C_2 product selectivity by temperature of OSs_1h; (d) C_2 product selectivity by temperature of Chinese CaO; (e) Hydrocarbon products selectivity at 750 °C; (f) Hydrocarbon products yield at 750 °C; (g) CH_4 conversion of samples at 750 °C over time; (h) C_2 (C_2H_4 and C_2H_6) product selectivity of samples at 750 °C over time

Fig. 5b to Fig. 5d show the importance of alkali metals in selecting desired products. According to several investigations, the presence and concentration of alkali elements impact product selectivity [5, 14, 15]. In addition, the strong basicity is also an important factor for oxygen mobility and oxygen defects. These defects are believed to increase the selective conversion of

methane into ethylene and help limit the nonselective oxidation of O^- [14, 19]. This was demonstrated by the experimental results in this study. The calcined samples from the oyster shells show significantly better selectivity for the main product compared to the Chinese CaO sample, even at the low temperature of 650 °C (Fig. 5b to Fig. 5d). Fig. 5e shows that the Air/OSs_0h sample has the highest C_{2+} hydrocarbon selectivity at 750 °C with the value of 70.3%. The selectivity of the Air/OSs_0h sample is higher than that of the other OSs samples because the elemental mapping and SEM results (Fig. 3) show that Air/OSs_0h existed in the form of small, evenly distributed, discrete particles. The Chinese CaO had the lowest value of 46.37%; indeed, this is because the Chinese or commercial CaO was refined and eliminated basicity impurities, so its basicity is lower than the OSs samples. In addition, the propylene selectivity of the Air/OSs_0h was twice as high as that of the other catalysts at 750 °C (Fig. 5e), reaching the value of 0.7%. This shows that the Air/OSs_0h sample is the most promising catalyst in this study, as clearly shown in the hydrocarbon yield chart in Fig. 5f.

All samples except for Air/OSs_0h were studied for stability and the results were shown in Fig. 5g to Fig. 5h. The data described CH_4 conversion at 750 °C over time, and hydrocarbon products selectivity at 750 °C show that CH_4 conversion of Chinese CaO was the highest (about 15%), followed by Oss_1h (10%), and Oss_0h (about 7%). Fig. 5g shows the CH_4 conversion value changed slightly over time. This shows that the samples maintained a stable conversion over time. The CH_4 conversion of the OSs_0h sample showed a decreasing trend, possibly due to the influence of $CaCO_3$ in this sample. The OSs_1h and the Chinese CaO tend to be stable, and the OSs_1h show almost no significant change in CH_4 conversion over time. As a result, CaO powder was synthesized from oyster shells that were as stable as commercial CaO powder. Fig. 5h shows that the selectivity for hydrocarbons decreased in the CaO samples synthesized from oyster shells. This decrease is likely related to the influence of temperature and carbon dioxide on the alkali metals present in these samples. The modification of alkali metals gradually reduced the selectivity of hydrocarbon products; overall, this reduction is not significant. Although the synthesis conditions in this work limited the study of the stability of the Air/OSs_0h sample, this sample is the most promising catalyst.

4. Conclusion

CaO powder was successfully synthesized under the surveyed conditions. The conditions in the oven are very harsh, so the surface area of the samples is low. Air/OSs_0h has a large surface area, so its conversion rate is approximately the same as that of commercial CaO samples. Due to the presence of alkali metals (Na and Mg) in the composition, the synthesized CaO samples from oyster shells exhibit superior selectivity for hydrocarbons. The influence of salt on the reaction can vary in different areas where oysters live and grow with a little or a lot of salt. Air/OSs_0h is a promising method for synthesizing catalysts suitable for the OCM process.

Acknowledgements

This work was performed at GeViCat center, Hanoi University of Science and Technology. This work has been supported by the RoHan Project funded by the German Academic Exchange Service (DAAD, No. 57315854 and 57560571) and the Federal Ministry for Economic Cooperation and Development (BMZ) inside the framework "SDG Bilateral Graduate school programme".

References

[1] P. Schwach, P. Xiulian, and B. Xinhe, Direct conversion of methane to value-added chemicals over heterogeneous catalysts: challenges and prospects, Chemical Reviews, vol. 117, iss. 13, pp. 8497–8520, May 2017. https://doi.org/10.1021/acs.chemrev.6b00715

[2] IEA, Driving Down Coal Mine Methane Emissions: A Regulatory Roadmap and Toolkit, OECD Publishing, Paris, 2023. https://doi.org/10.1787/9545d7b3-en

[3] T. Biswal, K. P. Shadangi, P. K. Sarangi, and R. K. Srivastava, Conversion of carbon dioxide to methanol: A comprehensive review, Chemosphere, vol. 298, Jul. 2022, Art. no. 134299. https://doi.org/10.1016/j.chemosphere.2022.134299

[4] V. Dieterich, A. Buttler, A. Hanel, H. Spliethoff, and S. Fendt, Power-to-liquid via synthesis of methanol, DME or Fischer–Tropsch fuels: a review, Energy and Environmental Science, vol. 13, iss. 10, pp. 3207–3252, Aug. 2020. https://doi.org/10.1039/D0EE01187H

[5] J. Liu, J. Yue, M. Lv, F. Wang, Y. Cui, Z. Zhang, and G. Xu, From fundamentals to chemical engineering on oxidative coupling of methane for ethylene production: a review, Carbon Resources Conversion, vol. 5, iss. 1, pp. 1–14, Mar. 2022. https://doi.org/10.1016/j.crcon.2021.11.001

[6] G. E. Keller and M. M. Bhasin, Synthesis of ethylene via oxidative coupling of methane: I. determination of active catalysts, Journal of Catalysis, vol. 73, iss. 1, pp. 9–19, Jan. 1982. https://doi.org/10.1016/0021-9517(82)90075-6

[7] Z. Stansch, L. Mleczko, M. Baerns, Comprehensive kinetics of oxidative coupling of methane over the La_2O_3/CaO catalyst, Industrial and Engineering Chemistry Research, vol. 36, iss. 7, pp. 2568–2579, Jul. 1997. https://doi.org/10.1021/ie960562k

[8] B. An, K. Ryu, Y. Kim, and S. Lee, Activation of methane to C_2 hydrocarbons over unpromoted calcium oxide catalysts, Bulletin of the Korean Chemical Society, vol. 28, iss. 6, pp. 1049–1052, Jun. 2007. https://doi.org/10.5012/bkcs.2007.28.6.1049

[9] D. S. Lima and O. W. Perez-Lopez, Oxidative coupling of methane to light olefins using waste eggshell as a catalyst, Inorganic Chemistry Communications, vol. 116, Jun. 2020, Art. no. 107928. https://doi.org/10.1016/j.inoche.2020.107928

[10] Imarc group, Oyster Market Report by Oyster Type (Cupped Oyster, Pacific Cupped Oyster, American Cupped Oyster, Penguin Wing Oyster, and Others), End User (Foodservice, Retail), Packaging Form (Fresh, Frozen, Canned, and Others), and Region 2024-2032, [Online]. Available: https://www.imarcgroup.com/oyster-market, Accessed on: 2023, Report ID: SR112024A3856.

[11] M. R. R. Hamester, P. S. Balzera, D. Becker, Characterization of calcium carbonate obtained from oyster and mussel shells and incorporation in polypropylene, Materials Research, vol. 15, iss. 2, pp. 204–208, Apr. 2012. https://doi.org/10.1590/S1516-14392012005000014

[12] K. S. P. Karunadasa, C. H. Manoratne, H. M. T. G. A. Pitawala, and R. M. G. Rajapakse, Thermal decomposition of calcium carbonate (calcite polymorph) as examined by in-situ high-temperature X-ray powder diffraction, Journal of Physics and Chemistry of Solids, vol. 134, pp. 21–28, Nov. 2019. https://doi.org/10.1016/j.jpcs.2019.05.023

[13] S. S. Parker, A. Long, C. Lhermitte, S. Vogel, M. Monreal, and J. M. Jackson, Thermophysical properties of liquid chlorides from 600 to 1600 K: melt point, enthalpy of fusion, and volumetric expansion, Journal of Molecular Liquids, vol. 346, Jan. 2022, Art. no. 118147. https://doi.org/10.1016/j.molliq.2021.118147

[14] Z. Fakhroueian, F. Farzaneh, and N. Afrookhteh, Oxidative coupling of methane catalyzed by Li, Na and Mg doped $BaSrTiO_3$, Fuel, vol. 87, iss. 12, pp. 2512–2516, 2008. https://doi.org/10.1016/j.fuel.2008.02.010

[15] V. H. Rane, S. T. Chaudhari, and V. R. Choudhary, Influence of alkali metal doping on surface properties and catalytic activity/selectivity of CaO catalysts in oxidative coupling of methane, Journal of Natural Gas Chemistry, vol. 17, iss. 4, 2008, pp. 313–320. https://doi.org/10.1016/S1003-9953(09)60001-3

[16] C. Matei, D. Berger, A. Dumbrava, M. D. Radu, and E. Gheorghe, Calcium carbonate as a silver carrier in composite materials obtained in green seaweed extract with topical applications. Journal of Sol-Gel Science and Technology, vol. 93, pp. 315–323, 2020. https://doi.org/10.1007/s10971-019-05145-6

[17] M. M. H. A. Omari, I. S. Rashid, N. A. Qinna, A. M. Jaber, and A. A. Badwan, Calcium carbonate, profiles of drug substances, excipients and related methodology, Profiles of Drug Substances, Excipients and Related Mehodology, vol. 41, 2016, pp. 31–132. https://doi.org/10.1016/bs.podrm.2015.11.003

[18] A. Roy and J. Bhattacharya, Microwave assisted synthesis of CaO nanoparticles and use in waste water treatment, International Journal of Nanotechnology and Applications, vol. 3, iss. 3, pp. 565–568, 2011.

[19] X. Gao, P. Cai, Z. Wang, X. Lv, and S. Kawi, Surface acidity/basicity and oxygen defects of metal oxide: impacts on catalytic performances of CO_2 reforming and hydrogenation reactions, Topics in Catalysis, vol. 66, pp. 299–325, 2023. https://doi.org/10.1007/s11244-022-01708-0